

Solvable model of driven matter with pinningGourab Kumar Sar^{1,*}, Dibakar Ghosh^{1,†} and Kevin O’Keeffe^{2,‡}¹*Physics and Applied Mathematics Unit, Indian Statistical Institute, 203 B. T. Road, Kolkata 700108, India*²*Senseable City Lab, Massachusetts Institute of Technology, Cambridge, Massachusetts 02139, USA*

(Received 15 June 2023; accepted 15 March 2024; published 9 April 2024)

We present a simple model of driven matter in a 1D medium with pinning impurities, applicable to magnetic domain walls, confined colloids, and other systems. We find rich dynamics, including hysteresis, reentrance, quasiperiodicity, and two distinct routes to chaos. In contrast to other minimal models of driven matter, the model is solvable: we derive the full phase diagram for small N , and for large N , we derive expressions for order parameters and several bifurcation curves. The model is also realistic. Its collective states match those seen in the experiments of magnetic domain walls.

DOI: [10.1103/PhysRevE.109.044603](https://doi.org/10.1103/PhysRevE.109.044603)**I. INTRODUCTION**

Driving matter through disordered environments has diverse applications in science. Magnetic domain walls and other quasiparticles may be driven off material defects and used as memory units in spintronics [1–4]. Electromagnetic colloids may be forced to self-assemble into cargo carriers for high-precision medicine [5–8]. The colloids may also be used to repair circuits [9], purify water [10], and shatter blood clots [11,12].

All these applications rely on our ability to predict how a given matter collective reacts to driving. To be concrete here, imagine a particle swarm being pushed around by an external field. We need to be able to predict the swarm’s movements, and how those movements change as we change parameters—to predict its collective dynamics and bifurcations. Predicting these however is hard, because of swarms’ numerous degrees of freedom and nonlinear particle interactions. It takes us into the world of nonequilibrium statistical mechanics and many-body dynamical systems where standard tools and techniques fail. Take magnetic domain walls. Each one obeys the integro-differential Landau-Lifshitz-Gilbert equation, so N obey a set of coupled such equations whose solution is virtually impossible. (For $N = 1, 2$ walls approximations such as the (q, ϕ) model [13,14] have been derived, but bifurcations and scaling beyond $N > 2$ is difficult [14,15].) And for magnetic colloids, because of the coupling to the host fluid, there is an extra Navier-Stokes type equation added to the mix. Vicsek-type models are sometimes used as approximations here [16–19], but are still largely intractable; order parameters and bifurcation are often computed numerically [16,18,20,21], leaving solvable models of driven matter scarce.

This paper helps close this research gap by introducing a model of driven matter which is solvable (in the sense that expressions for its order parameters and several of its bifurcation curves may be derived explicitly). Our approach is to study a deliberately simplified model which hopefully captures behavior with some universality, as opposed to a detailed model specific to magnetic particles or colloids. The model’s form is inspired from studies of coupled oscillators [22–26] which allows us to leverage new tools from that field to solve it.

II. MODEL

Consider N particles moving in a one dimensional (1D) periodic domain obeying

$$\dot{x}_i = E - b \sin(x_i - \alpha_i) + \frac{J}{N} \sum_j \sin(x_j - x_i) \cos(\theta_j - \theta_i), \quad (1)$$

$$\dot{\theta}_i = E - b \sin(\theta_i - \beta_i) + \frac{K}{N} \sum_j \sin(\theta_j - \theta_i) \cos(x_j - x_i). \quad (2)$$

Here $(x_i, \theta_i) \in (\mathbb{S}^1, \mathbb{S}^1)$ where \mathbb{S}^1 is the unit circle are the i th particle’s position and phase, respectively. This phase could represent the orientation of a particle, the (in-plane) orientation of an electric or magnetic dipole, or be associated with an internal rhythm, like the chemical oscillation on the surface of an autocatalytic particle [27]. Domain disorder is modeled by the $b \sin(\cdot)$ terms, which pin x_i and θ_i to sites α_i, β_i (we do not consider thermal disorder), and external driving by the E terms. The Kuramoto $\sin(\cdot) \cos(\cdot)$ terms capture particle interactions. For the phases θ_i , this creates synchronization which depends on the distance, for the positions x_i , aggregation which depends on the particles’ phases, natural choices of interaction because they occur in diverse systems such as Janus particles [28] and Quincke rollers [29]. We ignore excluded volume interactions for simplicity.

*mr.gksar@gmail.com

†diba.ghosh@gmail.com

‡kevin.p.okeeffe@gmail.com

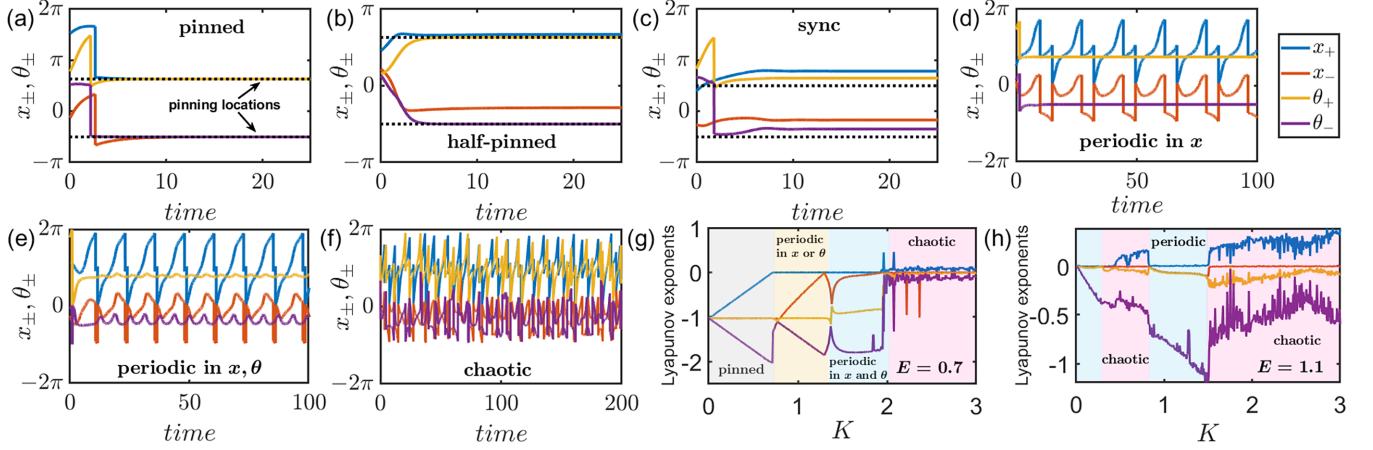


FIG. 1. States and bifurcations for $J = -K$. (a) Pinned ($E = 0.4, K = 0.5$), (b) half-pinned ($E = 0.4, K = 1.1$), (c) sync ($E = 0.4, K = 2.1$), (d) periodic in x , fixed in θ ($E = 0.7, K = 1.0$), (e) periodic in both x and θ ($E = 0.7, K = 1.8$), (f) chaotic ($E = 1.1, K = 1.0$). Lyapunov exponents highlight the bifurcations for two different values of E . (g) $E = 0.7$, (h) $E = 1.1$. The system is integrated with $(dt, T) = (0.01, 100)$ using an RK4 method.

III. SMALL N REGIME

We explore the little N limit with a case study of $N = 2$ particles. The physical system we have in mind here is two magnetic domain walls moving on circular race track memory [30], similar to recent experiments [31], (there, however, the spatial domain was a straight line; here it is periodic, $x \in \mathbb{S}^1$). For simplicity, we study symmetric pinning sites $(\alpha_1, \alpha_2) = (\beta_1, \beta_2) = (0, \pi)$ (which may be appropriate for periodic substrates [19,32]). Setting $b = 1$ without loss of generality and moving to coordinates $(x_{\pm}, \theta_{\pm}) = ((x_1 \pm x_2)/2, (\theta_1 \pm \theta_2)/2)$ yields

$$\dot{x}_+ = E - \cos x_+ \sin x_-, \quad (3)$$

$$\dot{x}_- = -\sin x_+ \cos x_- - \frac{J}{2} \sin 2x_- \cos 2\theta_-, \quad (4)$$

$$\dot{\theta}_+ = E - \cos \theta_+ \sin \theta_-, \quad (5)$$

$$\dot{\theta}_- = -\sin \theta_+ \cos \theta_- - \frac{K}{2} \sin 2\theta_- \cos 2x_-. \quad (6)$$

The behavior of the model divides into two cases depending on the relative sign of J and K . We present the opposite sign case first because it contains the most relevant physics.

A. Opposite sign coupling

We start with setting $J = -K$ for ease since the magnitude of J does not change the overall phenomena which will be discussed later in this section. First, we develop some intuition for our system by visualizing its dynamics. Imagine the particles as moving dots in the (x, θ) plane with periodic boundary conditions (equivalently, the torus). Limit case dynamics are easy to picture. When the driving dominates $E \gg b, K$, the particles will be swept around the plane in uniform rotations. When the pinning is large $b \gg E, K$, they will freeze into their pinning sites $x_i = \theta_i = \alpha_i$. And when the coupling wins out $K \gg b, E$, they will unstuck from α_i and lock into synchrony (since $J = -K$, it will not be straightforward synchrony $x_1 = x_2, \theta_1 = \theta_2$, which we expect for $J = K$, but some type of

antisync). But what happens when the three effects have comparable strengths $b \approx K \approx E$? And how do the various states arise and disappear as the parameters change?

To answer these questions, we ran numerical experiments. Figure 1 shows our results, but before we talk through them, one should look at the bifurcation diagram in Fig. 2 which shows where each collective state occurs in parameter space. Having this birds eye view of the system's dynamics in mind as you read will help you follow the story. Supplemental Movie 1 [33] also presents a live demo of our experiments which is also useful to watch at this point.

To begin, we realized the pinned state—a natural “ground state” to perturb around—by turning off the driving $E = 0$ and setting the phase coupling K small. Fig. 1(a) shows time series of the coordinates x_{\pm}, θ_{\pm} relaxing from random

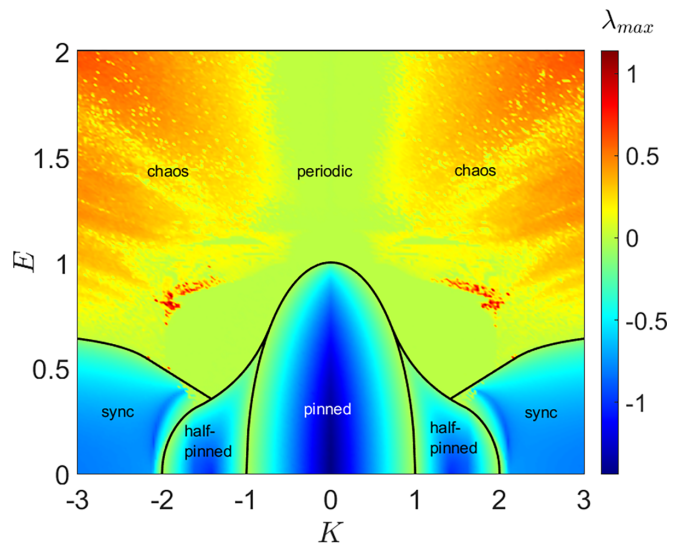


FIG. 2. Bifurcation diagram for $N = 2$ particles for $J = -K$. Black lines denote theoretical predictions, and colors signify the largest Lyapunov exponent. In the periodic and chaotic parameter regions, bistability was sometimes observed.

initial conditions to the pinning sites, depicted as dotted lines (in the \pm coordinates, the sites are $\alpha_{\pm} = \pm\pi/2$). Then we gradually increased K , expecting the particles to synchronize in the sense of minimizing their space differences x_{-} and phase differences θ_{-} . (Note, however, that since driving is turned off, we do not expect the particles to oscillate here, we expect them to just shift to a new fixed point.) We find two transitions. First, a half-pinned state emerges, where θ_{\pm} stay pinned, but the phases x_{\pm} are locked into a new sync fixed point [Fig. 1(b)]. Notice the θ_{\pm} line settles onto the pinning sites (dotted line), but x_{\pm} does not. In the second transition, the remaining coordinates depin and a full sync state is realized where all four coordinates lie off the pinning sites [Fig. 1(c)].

We have thus found three static states with the driving turned off E : pinned, half-pinned, and sync. As we turn on the driving $E > 0$, how much can each state withstand before x_{\pm} , θ_{\pm} unlock and start moving? Look at the bifurcation diagram in Fig. 2. For $E \lesssim 0.25$, the pinned \rightarrow half-pinned \rightarrow sync transition persists, but for larger driving $E \approx 0.5$, some periodic states (green region near the solid black boundary) arise between the half-pinned and sync states. Here, either two of the four coordinates (x_{\pm} , θ_{\pm}) oscillate, the others remaining fixed [Fig. 1(d)], or all four coordinates oscillate [Fig. 1(e)]. For larger driving till $E \approx 0.8$, the pinned state morphs directly into periodicity, which in turn undergoes an intermittency transition to chaos (orangish region highlighted in the figure) depicted in Fig. 1(f). Finally, for $E > 1$, the static states vanish and the dynamic ones become reentrant: the system flip flops between chaotic and periodic motion, then settles into chaos (bistability between the two states was sometimes observed).

To confirm the motion was chaotic, we computed a heat map of Lyapunov exponents λ_{\max} in the (K, E) plane and saw $\lambda_{\max} > 0$ where expected. We also compute power spectra which indicate the chaotic transition is of the intermittent type. In Fig. 3, we analyze in detail the chaotic behavior by plotting the bifurcation diagram, power spectra, and time series for $J = -K$ with $N = 2$ swarms. Chaotic behavior emerges when the driving strength E increases. The route is intermittent which can be seen from the power spectral density (PSD) plot. For convenience, we also plot the Lyapunov exponents $\lambda(K)$ to show the bifurcation sequence at $E = 0.7$ and $E = 1.1$ in Figs. 1(g) and 1(h).

Now we turn to analysis. We derive fixed-point expressions for x_{\pm} , θ_{\pm} in the static states and derive their bifurcation curves drawn as black lines in Fig. 2. We find the fixed points by setting the RHS of Eqs. (3)–(6) to zero. Then we eliminate (x_{-} , θ_{-}) using Eqs. (3) and (5) and substitute the result into Eqs. (4) and (6):

$$\sqrt{1 - E^2 \sec^2 x_{+}} \left(\frac{EK(2E^2 \sec^2 \theta_{+} - 1)}{\cos x_{+}} - \sin x_{+} \right) = 0, \quad (7)$$

$$\sqrt{1 - E^2 \sec^2 \theta_{+}} \left(\frac{EK(2E^2 \sec^2 x_{+} - 1)}{\cos \theta_{+}} - \sin \theta_{+} \right) = 0. \quad (8)$$

The system has form $AB = CD = 0$, implying four sets of fixed points. When $(A, C) = (0, 0)$ we get the pinned state. When $(A, D) = (0, 0)$ or $(B, C) = (0, 0)$ we get the half-

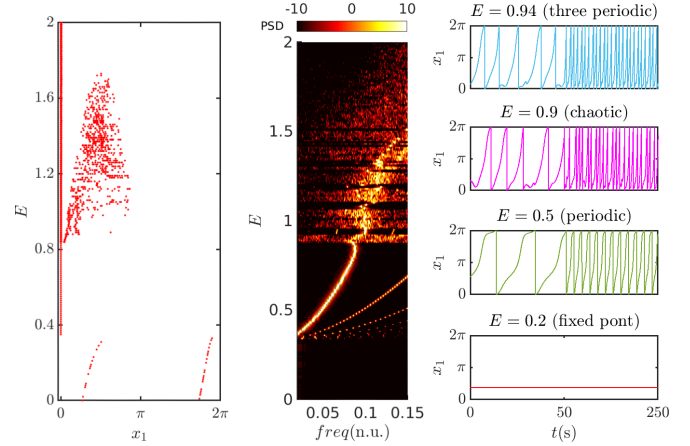


FIG. 3. Bifurcation diagram, power spectral density and time series. $K = -J = -1.5$. Simulation is performed with $N = 2$ swarms. For plotting the bifurcation diagram we have simulated our model for $T = 2000$ time units with step-size $dt = 0.01$ by RK4 method. Then last 5% data were considered and the local minimum was plotted. The same numerics were used for the PSD. The time series of x_1 are shown for four different values of E over $T = 250$ time units starting from the initial time $t = 0$.

pinned state (in the one x_i stays pinned, θ_i syncs, in the other the reverse), and when $(B, D) = (0, 0)$ we get the sync state. We now analyze each state one-by-one. The overall strategy is simple: the fixed points, and then determine their stability by linearization, but the calculations themselves are quite involved with long, many-term equations [for example, see Eqs. (A42)–(A46)]. We defer some of the more winding calculations to the Appendix.

1. Pinned state

$(A, C) = (0, 0)$ corresponds to the “pinned” state defined by

$$\sqrt{1 - E^2 \sec^2 x_{+}} = 0, \quad (9)$$

$$\sqrt{1 - E^2 \sec^2 \theta_{+}} = 0, \quad (10)$$

which have solution

$$x_{+} = \pm \cos^{-1} \pm E, \quad (11)$$

$$x_{-} = \pm \frac{\pi}{2}, \quad (12)$$

$$\theta_{+} = \pm \cos^{-1} \pm E, \quad (13)$$

$$\theta_{-} = \pm \frac{\pi}{2}. \quad (14)$$

There are 16 total solutions, corresponding to the permutation induced by the various \pm 's. Notice these only exist for $E \leq 1$. Only four are stable:

$$(x_{+}, x_{-}, \theta_{+}, \theta_{-}) = (\cos^{-1}(-E), -\pi/2, \cos^{-1}(-E), -\pi/2), \quad (15)$$

$$\text{or } (\cos^{-1}(-E), -\pi/2, -\cos^{-1}(E), \pi/2), \quad (16)$$

$$\text{or } (-\cos^{-1}(E), \pi/2, \cos^{-1}(-E), -\pi/2), \quad (17)$$

$$\text{or } (-\cos^{-1}(E), \pi/2, -\cos^{-1}(E), -\pi/2). \quad (18)$$

The eigenvalues are simply found using Mathematica,

$$\lambda = -\sqrt{1-E^2}, \sqrt{1-E^2} - K, \quad (19)$$

both with multiplicity two. Recall that fixed points exist only when $E \leq 1$, which means one of the two λ is always negative. The second one become unstable via a zero-eigenvalue bifurcation at

$$E_{c1} = \sqrt{1-K^2}, \quad (20)$$

which defines the stability boundary of the state (black curve in Fig. 2)

2. Half-pinned state

This state is defined by a symmetric pair of fixed points: when x_i stays pinned and θ_i syncs, or the reverse. In the above notation, these correspond to $(A, D) = (0, 0)$ and $(B, C) = (0, 0)$. We study the $(A, D) = (0, 0)$ without loss of generality, given by

$$\sqrt{1-E^2 \sec^2 x_+} = 0, \quad (21)$$

$$\sqrt{1-E^2 \sec^2 \theta_+} \times (EK \sec \theta_+ (2E^2 \sec^2 x_+ - 1) - \sin \theta_+) = 0. \quad (22)$$

Using Mathematica, we find 32 solutions to these, of which 4 are stable. These 4 fixed points have the form

$$x_+ = -\cos^{-1}(-E), \quad (23)$$

$$x_- = -\frac{\pi}{2}, \quad (24)$$

$$\theta_+ = \cos^{-1} \left(-\frac{\sqrt{1-\sqrt{1-4E^2K^2}}}{\sqrt{2}} \right), \quad (25)$$

$$\theta_- = -\sin^{-1} \left(\frac{\sqrt{2}E}{\sqrt{1-\sqrt{1-4E^2K^2}}} \right). \quad (26)$$

Finding the stability of these is harder. The Jacobian matrix yields eigenvalues $\lambda_1, \lambda_2, \lambda_3, \lambda_4$ whose expressions are daunting. See Appendix A for details. Solving $\lambda_3 = 0$ and removing the square roots by successive squaring however leads to see something cleaner

$$4E^4(2EK-1)(2EK+1)(E^2+K^2-1) \times ((2E^2K+K)^2+3(E^2-1)) = 0. \quad (27)$$

From this we can peel off the relevant stability branch

$$E_{c2} = -\frac{1}{2K}. \quad (28)$$

Solving $\lambda_2 = 0$ gives us the other part of the boundary

$$E_{c3} = \frac{\sqrt{-K^4+5K^2-4}}{3K}. \quad (29)$$

Together, E_{c2}, E_{c3} gives the boundary of the half-pinned state. They intersect at $K^* = \sqrt{5/2}$. Crossing the boundary again triggers a zero-eigenvalue bifurcation.

3. Sync state

This corresponds to the fixed point $(B, D) = (0, 0)$,

$$EK \sec x_+ (2E^2 \sec^2 \theta_+ - 1) - \sin x_+ = 0, \quad (30)$$

$$EK \sec \theta_+ (2E^2 \sec^2 x_+ - 1) - \sin \theta_+ = 0. \quad (31)$$

The fixed-point expressions as the solution of the above equations are so long as to not be enlightening to display here. So we place the entire analysis of the sync state in the Appendix A. Our ultimate results are the stability boundaries of the state, which, as before, come in two pieces,

$$E_{c4} = \frac{K}{4}, \quad (32)$$

$$E_{c5} = \frac{1}{2} \sqrt{\frac{K(\sqrt{K^2-4}+K)-1}{K^2}}. \quad (33)$$

E_{c4} and E_{c5} meet at $K^* = \sqrt{2(1+\sqrt{2})}$. These theoretical predictions are the thick black curves in the bifurcation diagram Fig. 2.

This completes our analysis.

B. Same-sign coupling

Now we turn from opposite to same sign coupling $J = K$. The analysis is similar to the above, but surprisingly, gets much easier. The governing equations read

$$\dot{x}_+ = E - \cos x_+ \sin x_-, \quad (34)$$

$$\dot{x}_- = -\sin x_+ \cos x_- - \frac{K}{2} \sin 2x_- \cos 2\theta_-, \quad (35)$$

$$\dot{\theta}_+ = E - \cos \theta_+ \sin \theta_-, \quad (36)$$

$$\dot{\theta}_- = -\sin \theta_+ \cos x_- - \frac{K}{2} \sin 2\theta_- \cos 2x_-. \quad (37)$$

There are four fixed points like last time, but only the pinned and half-pinned are stable. So those are the only two states we analyze.

1. Pinned

The fixed points are

$$x_+ = \pm \cos^{-1}(\mp E), \quad (38)$$

$$x_- = \pm \frac{\pi}{2}, \quad (39)$$

$$\theta_+ = \pm \cos^{-1}(\mp E), \quad (40)$$

$$\theta_- = \pm \frac{\pi}{2}, \quad (41)$$

which has a saddle node (SN) at $E = \sqrt{1-K^2}$ ($K < 0$) and a saddle node infinite period (SNIPER) at $E = 1$ (Fig. 4). It is to be noted that, pinned state is the only stable steady solution for $K > 0$. The other steady state exists for $K < 0$ and we derive its stability next.

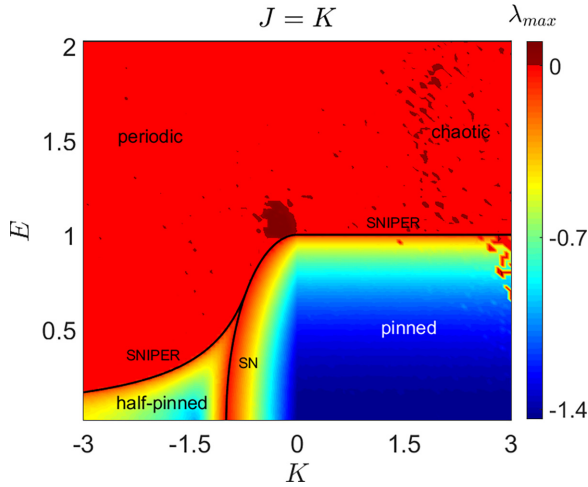


FIG. 4. Bifurcation diagrams in (K, E) space for $J = K$. Colors indicate the largest Lyapunov exponent (λ_{\max}) of the system. Black curves denote analytically calculated stability boundaries. SN stands for saddle node bifurcation and SNIPER stands for saddle node infinite period bifurcation.

2. Half-pinned

Here the fixed points are

$$x_+ = \cos^{-1}(-E), \quad (42)$$

$$x_- = -\frac{\pi}{2}, \quad (43)$$

$$\theta_+ = \sec^{-1}\left(-\frac{\sqrt{2}}{\sqrt{1 - \sqrt{1 - 4E^2K^2}}}\right), \quad (44)$$

$$\theta_- = \sin^{-1}\left(\frac{\sqrt{2}E}{\sqrt{1 - \sqrt{1 - 4E^2K^2}}}\right). \quad (45)$$

From the eigenvalues at this fixed point (see Appendix B) the stability boundary is found as

$$E_{c6} = -\frac{1}{2K}. \quad (46)$$

At this boundary a SNIPER bifurcation takes place which results into a periodic orbit. See Fig. 4 for details. The black curves are the analytically calculated stability boundaries.

C. Model robustness

Let us take stock of our findings. We find three static states, a family of periodic states, chaos, and various interstate transitions. Now we show our case study of even coupling $J = -K$ and symmetric pinning $(\alpha_1, \alpha_2) = (0, \pi)$ is representative of the full coupling $J = -cK$, $c \neq 1$ and asymmetric coupling $(0, a\pi)$ for $a \neq 1$ regime. Figures 5(a) and 5(b) show the same physics, in the sense of qualitatively identical bifurcations diagrams, are found for $J = -\sqrt{3}K$, $J = -K/\sqrt{3}$. The same was true when we relaxed the symmetric pinning by defining $(\alpha_1, \alpha_2) = (0, a\pi)$ and tuning $a \leq 1$ (note we can set $\alpha_0 = 0$ without loss of generality), although in this case the bifurcations of the static states get richer; Fig. 5(c) shows the half-pinned and sync states become reentrant. Most of the

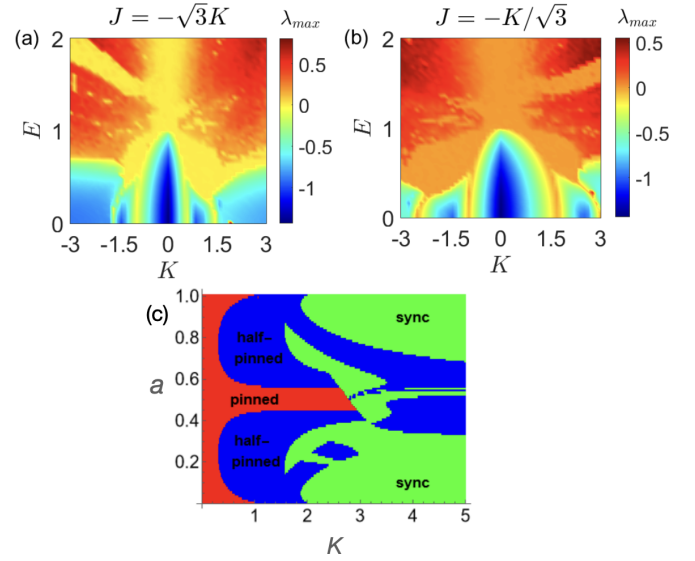


FIG. 5. Model Robustness. (a), (b) Bifurcation diagrams for noneven coupling $J = -cK$ where $c = \sqrt{3}, 1/\sqrt{3}$ are qualitatively identical to the even coupling $J = -K$ case study presented in the text. (c) Bifurcation diagram for static states when the pinning is relaxed from being perfected symmetric $(\alpha_1, \alpha_2) = (0, \pi)$ to asymmetric $(\alpha_1, \alpha_2) = (0, a\pi)$ for $0 \leq a \leq 1$. Notice the half-pinned and sync states become reentrant; for $a \approx 0.8$ and increasing K , the system transitions as pinned \rightarrow half-pinned \rightarrow sync \rightarrow half-pinned \rightarrow sync. We have set $E = 0.1$ here.

collective states also appear for same-sign coupling $J = K$, albeit with a different bifurcation structure.

IV. MATCH TO MAGNETIC DOMAIN WALLS

Our hope was that these states capture real-world behavior. They do. Figure 6 shows they mimic the behavior found in a recent study [31] of a pair magnetic domain walls. Briefly, their setup is this. Each wall is free to move in the x direction, and one wall is slightly higher than the other in the y direction, so that they do not collide. Then each wall i may be characterized by a single spatial degree of freedom $x_i \in \mathbb{R}^1$ and also a phase $\theta_i \in \mathbb{S}^1$ corresponding to the effective magnetic dipole vector of the wall; thus the walls fall into our model class (see Ref. [31] for more details on the phase θ_i). The walls begin pinned at fixed points (x_i^*, θ_i^*) . Then an external magnetic field is turned on, which induces their positions x_i and θ_i to unlock and interact. The top row of Fig. 6, taken from Ref. [31], shows the resulting dynamics for different parameters with scatter plots of the dipole vectors for each wall (m_1, m_2) . These m_i relate to the phase via $m_i \propto \sin \theta_i$, as indicated by the axes labels. Notice the walls settle into simple periodic behavior or more complex dynamics represented by Lissajous curves and point clouds. The middle and bottom rows show our model reproduces these states for the both the $J = -K$ and $J = K$ cases.

V. LARGE N REGIME

We analyzed the $N \rightarrow \infty$ states for $J = K$ in a previous work [34]. We summarize the results here for convenience

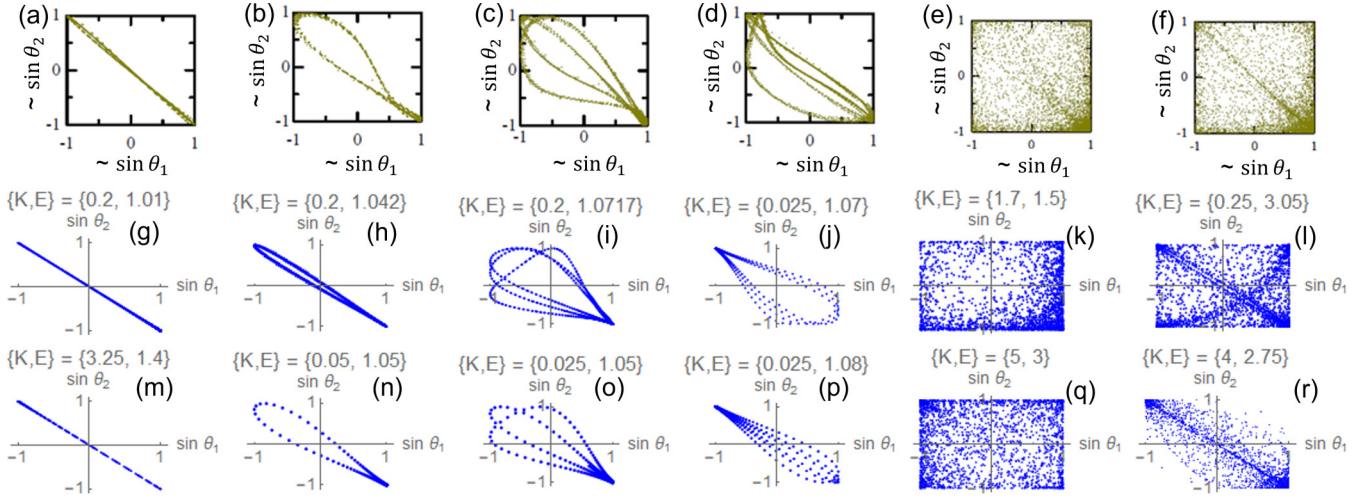


FIG. 6. Match to micromagnetic simulations of two domain walls. Top row (a)–(f), high resolution micromagnetic simulations from Ref. [31]. Middle row (g)–(l), $J = -K$ and bottom row (m)–(r), $J = K$ model Eqs. (1) and (2). Numerical parameters: $(dt, T) = (0.25, 200)$. Initial (x_i, θ_i) were drawn uniformly at random from $[0, 2\pi]$. Multistability was sometimes observed. Reprinted Supplementary Figs. 7 and 8 with permission from Hrabec *et al.* [*Phys. Rev. Lett.* **120**, 227204 (2018)]. Copyright (2023) by the American Physical Society.

(we wanted a single paper to house both the large and little N limit). We also add some new results about the $N \rightarrow \infty$ regime, namely an analysis of a 2D model where $x \in S^2$.

A. Summary of previous results

How does the behavior of the model change as $N \rightarrow \infty$? A surprise for $N \gg 1$ is that the opposite coupling $J = -K$ case gets simpler. The half-pinned and sync states disappear, leaving just the pinned and unsteady states (Fig. 7). We used linearly spaced pinning $\alpha_i = 2\pi i/N$ here to facilitate analysis (randomly chosen α_i, β_i produce similar results [34]).

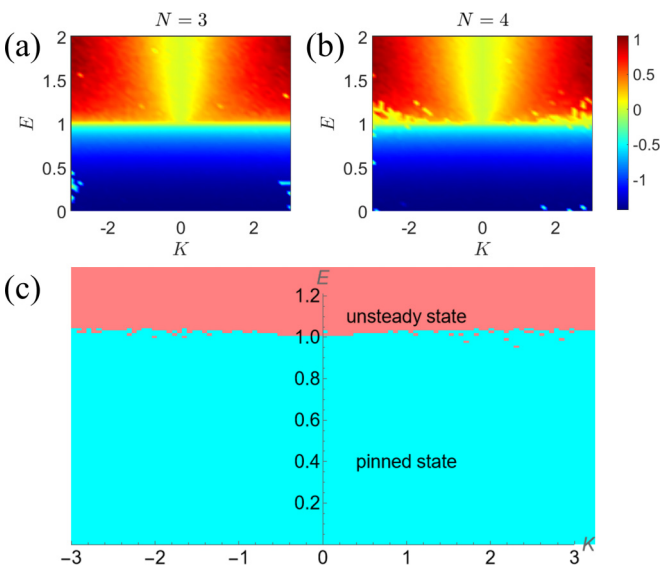


FIG. 7. Large N limit for $J = -K$. K - E space for (a) $N = 3$, (b) $N = 4$, and (c) $N \gg 1$. Notice the $N = 3, 4$ plots are much different to the $N = 2$ plot shown in the main text. Instead, they resemble the $N \rightarrow \infty$ plot shown in (c) where we use $N = 100$.

Dynamics for same-sign coupling $J = K$, in contrast, get richer. Figure 8(a) shows the pinned state (blue dots) persists, but now a new antipinned state (red stars) arises where neighboring particles are shifted by an amount $x_{i+1} - x_i = \theta_{i+1} - \theta_i = \Delta(K)$. Figure 8(b) shows the large N analog of the sync state with particles bunching into two sync clusters. New periodic behavior is observed, along with quasiperiodicity, and the route to chaos is now via period doubling. Supplemental Movies 2 and 3 [33] depict the evolution of all the states.

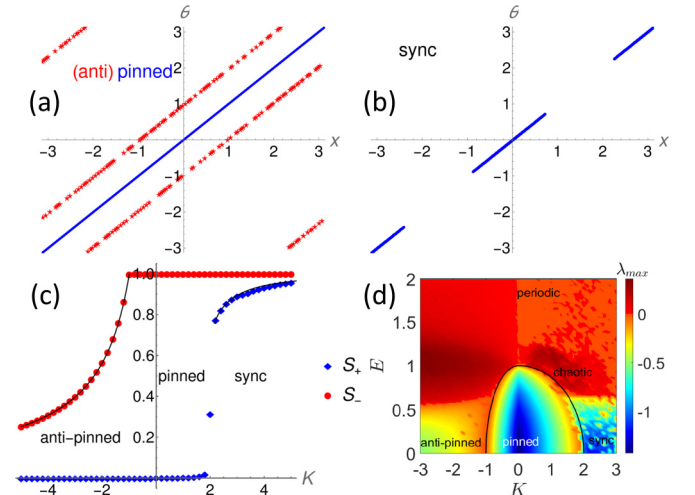


FIG. 8. Large N limit for $J = K$. (a) Pinned state (blue dots, $K = 1$) and antipinned state (red stars, $K = -2$) plotted on same graph to save space for $E = 0$ and $N = 200$ particles. (b) Sync state for $(K, E) = (3, 0)$. (c) Order parameters for $E = 0$. (d) Bifurcation diagram in (K, E) space. Black curves show theoretical predictions. Colors denote Lyapunov exponents, computed using $N = 10$ particles, which well approximated the $N \gg 1$ limit (simulations for larger N were prohibitive).

As for analysis, the critical coupling for the antipinned state is $E_c = \sqrt{1 - K^2}$, found using a self-consistency analysis, and for the pinned state is $E_c = \sqrt{1 - K^2/4}$, found using a variational argument [35]. These are the sides of the lopsided bell in the bifurcation diagram Fig. 8(d). We also derived expressions for the order parameters

$$W_{\pm} = S_{\pm} e^{i\Phi_{\pm}} = \frac{1}{N} \sum_j e^{i(x_j \pm \theta_j)}. \quad (47)$$

In the split phase wave,

$$S_- = -\frac{1}{3} + \frac{K^4 + (\Gamma_1 + 3\sqrt{3}\sqrt{\Gamma_2})^{2/3}}{3K^2(\Gamma_1 + 3\sqrt{3}\sqrt{\Gamma_2})^{1/3}}, \quad (48)$$

where

$$\Gamma_1 := -27(E^2 - 1)K^4 - K^6, \quad (49)$$

$$\Gamma_2 := (E^2 - 1)K^8(27E^2 + 2K^2 - 27). \quad (50)$$

In the sync state, we derived a pair of self-consistency equations for S_+ ,

$$-2 \sin\left(\frac{\xi}{2} - \alpha\right) + KS_+ \sin(\Phi_+ - \xi) = 0, \quad (51)$$

$$S_+ e^{i\Phi_+} = \frac{1}{2\pi} \int_0^{2\pi} e^{i\xi(\alpha)} d\alpha, \quad (52)$$

where $\xi_i := x_i - \theta_i$ which we solved numerically. We must solve Eq. (51) for the fixed points $\xi^*(\alpha)$ then plug them into Eq. (52) to find S_+ . First we set $\Phi_+ = 0$ without loss of generality. Then by applying various trig identities to Eq. (51) we arrive fourth-order polynomial in $\cos \xi^*$ and plug the roots into Eq. (52), which when $\Phi_+ = 0$ reads $S_+ = \int \cos(\xi^*(\alpha)) d\alpha$. Then we computed the integral over α numerically. Figure 8(c) shows these $S_{\pm}(K)$ match simulations and distinguish between the static states; in the pinned state $(S_+, S_-) = (1, 0)$ trivially by subbing $x_i = \theta_i$ into the definition for S_{\pm} Eq. (47). There is also a small region of hysteresis (not visible in the graph) between the pinned and sync states [34].

B. New results: Two-dimensional model

Recall that all our results so far were for one spatial (and circular) dimension, $x \in \mathbb{S}^1$. We were curious if the states persisted when the motion was two dimensional. Thus, we present a preliminary study of the following model:

$$\dot{x}_i = E - b \sin(x_i - \alpha_{x_i}) + \frac{J_x}{N} \sum_j \sin(x_j - x_i) \cos(\theta_j - \theta_i), \quad (53)$$

$$\dot{y}_i = E - b \sin(y_i - \alpha_{y_i}) + \frac{J_y}{N} \sum_j \sin(y_j - y_i) \cos(\theta_j - \theta_i), \quad (54)$$

$$\dot{\theta}_i = E - b \sin(\theta_i - \beta_i) + \frac{K}{N} \sum_j \sin(\theta_j - \theta_i) \times (\cos(x_j - x_i) + \cos(y_j - y_i)), \quad (55)$$

where $(x_i, y_i, \theta_i) \in (\mathbb{S}^1, \mathbb{S}^1, \mathbb{S}^1)$. Here x_i, y_i are the positions, and θ_i is the phase.

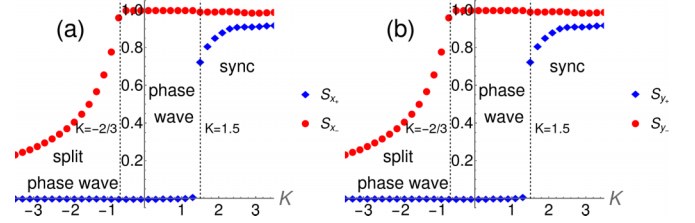


FIG. 9. Emerging states of the 2D model. We have fixed $E = 0$, $b = 1$, $J_x = J_y = K$ and $\alpha_{x_i} = \alpha_{y_i} = \beta_i = 2\pi i/N$. (a) Order parameters S_{x_+} (blue diamonds) and S_{x_-} (red dots). (b) Order parameters S_{y_+} (blue diamonds) and S_{y_-} (red dots). $(dt, T, N) = (0.5, 500, 1000)$. Last 50% data were taken to calculate the order parameters. Initially, x_i, y_i , and θ_i are chosen randomly from $[0, 2\pi]$.

Numerics show the model indeed supports 2D analogues of three static states (sync, phase wave, and split phase wave) as well as the nonsteady states. Figure 9 shows the generalized order parameters

$$W_{x_{\pm}} = S_{x_{\pm}} e^{i\Phi_{x_{\pm}}} = \frac{1}{N} \sum_j e^{i(x_j \pm \theta_j)}, \quad (56)$$

$$W_{y_{\pm}} = S_{y_{\pm}} e^{i\Phi_{y_{\pm}}} = \frac{1}{N} \sum_j e^{i(y_j \pm \theta_j)} \quad (57)$$

can discern the static states [just like Fig. 8(c) in the 1D case]. Below, we derive the stability thresholds for the phase wave and split phase waves. We leave an explorations of the sync state and unsteady states for future work.

1. Phase-wave state

For $J_x = J_y = K$, the potential function can be written as

$$\begin{aligned} V(x_{\alpha}, \theta_{\alpha}) = & -E \int_0^{2\pi} x_{\alpha} d\alpha - E \int_0^{2\pi} y_{\alpha} d\alpha \\ & -E \int_0^{2\pi} \theta_{\alpha} d\alpha - \int_0^{2\pi} \cos(\alpha - x_{\alpha}) d\alpha \\ & - \int_0^{2\pi} \cos(\alpha - y_{\alpha}) d\alpha - \int_0^{2\pi} \cos(\alpha - \theta_{\alpha}) d\alpha \\ & - \frac{K}{4\pi} \int_0^{2\pi} \int_0^{2\pi} [\cos(x_{\beta} - x_{\alpha}) + \cos(y_{\beta} - y_{\alpha})] \\ & \times \cos(\theta_{\beta} - \theta_{\alpha}) d\alpha d\beta, \end{aligned} \quad (58)$$

$$\Gamma(\eta) = \frac{d^2}{d\epsilon^2} V(x_{\alpha}(\epsilon))|_{\epsilon=0}, \quad (59)$$

becomes

$$\begin{aligned} \Gamma(\eta) = & 3\sqrt{1 - E^2} \int_0^{2\pi} \eta_{\alpha}^2 d\alpha \\ & + \frac{K}{\pi} \int_0^{2\pi} \int_0^{2\pi} (\eta_{\beta} - \eta_{\alpha})^2 \cos(2\beta - 2\alpha) d\alpha d\beta. \end{aligned} \quad (60)$$

Analyzing this quadratic form, we get the stability criterion for the phase-wave state as $\frac{3}{2}\sqrt{1 - E^2} - K > 0$. For $E = 0$, we get $K_{c1} = 1.5$ which is found to be satisfied from Fig. 9.

2. Split phase-wave state

In the split phase-wave state, the fixed points can be written down as

$$x_i = y_i = \alpha_i + \sin^{-1}(E) + (-1)^i \Delta, \quad (61)$$

$$\theta_i = \beta_i + \sin^{-1}(E) + (-1)^{i-1} 2\Delta. \quad (62)$$

We simplify our model by converting the trigonometric functions to complex exponentials,

$$\begin{aligned} \dot{x}_i = & E - \sin(x_i - \alpha_i) + \frac{K}{2} S_{x_+} \sin(\Phi_{x_+} - (x_i + \theta_i)) \\ & + \frac{K}{2} S_{x_-} \sin(\Phi_{x_-} - (x_i - \theta_i)), \end{aligned} \quad (63)$$

$$\begin{aligned} \dot{y}_i = & E - \sin(y_i - \alpha_i) + \frac{K}{2} S_{y_+} \sin(\Phi_{y_+} - (y_i + \theta_i)) \\ & + \frac{K}{2} S_{y_-} \sin(\Phi_{y_-} - (y_i - \theta_i)), \end{aligned} \quad (64)$$

$$\begin{aligned} \dot{\theta}_i = & E - \sin(\theta_i - \beta_i) + \frac{K}{2} S_{x_+} \sin(\Phi_{x_+} - (x_i + \theta_i)) \\ & - \frac{K}{2} S_{x_-} \sin(\Phi_{x_-} - (x_i - \theta_i)) \\ & + \frac{K}{2} S_{y_+} \sin(\Phi_{y_+} - (y_i + \theta_i)) \\ & - \frac{K}{2} S_{y_-} \sin(\Phi_{y_-} - (y_i - \theta_i)). \end{aligned} \quad (65)$$

We solve the $E = 0$ case for simplicity. From the definitions of S_{x_-} and S_{x_+} , we get from Eqs. (61) and (62) that $S_{x_-} = S_{y_-} = \cos 3\Delta$. Further, by substituting Eqs. (61) and (62) into Eq. (63), and equating with zero, we get

$$\sin \Delta = K \frac{S_{x_-} \sqrt{1 - S_{x_-}^2}}{2}. \quad (66)$$

By using the identity $\cos 3\Delta = 4\cos^3 \Delta - 3\cos \Delta$ and after simplification we derive the following polynomial equation for S_{x_-} ,

$$\begin{aligned} -K^6 S^{12} + 3K^6 S^{10} - 3K^6 S^8 + K^6 S^6 - 6K^4 S^8 + 12K^4 S^6 \\ - 6K^4 S^4 - 9K^2 S^4 + 9K^2 S^2 + 4S^2 - 4 = 0. \quad (S = S_{x_-}) \end{aligned} \quad (67)$$

Mathematica could solve the equation and we find that the split phase-wave state becomes unstable at $K_{c2} = -2/3$ through a transcritical bifurcation.

VI. DISCUSSION

The reaction of particulate matter to external driving is crucial for applications yet difficult to understand theoretically. This paper sheds light on this class of dynamics with a toy model tractable in both the low and large N limit—moreover, the intermediary N regime is surprisingly well approximated by the $N \rightarrow \infty$ model; Figs. 7 and 10 show as few as $N \approx 4$ particles give the same physics. The model also captures the behavior of real-world systems such as magnetic domain walls

(Fig. 6), Japanese tree frogs [36] and Janus matchsticks [37] [both realize the antipinned state Fig. 8(a)]. We also suspect its chaos may be connected to the active turbulence of biological microswimmers [38], since the swimmers contain the same basic physics as the model: driving and emergence in environments with pinning.

Given this balance between solvability and realism, we wonder if the model ‘could be the Kuramoto model’ for this class of driven matter, by which we mean the simplest, representative model in a universality class. Future work could explore this conjecture by deriving our model from a physically rigorous model. Start with, say, the Landau-Lifshitz-Gilbert equations for magnetic particles, exploit a small quantity like a weak coupling limit or a separation of time scales using a perturbative method [39], and see if our model or something close to it pops out. This was the way the Kuramoto model itself was derived—starting with a general reaction diffusion equation and simplifying using phase reduction methods—and is the source, so to speak, of its universality [39].

Our model could guide experimental work on systems of magnetic domains walls and other particles [31,40]. Chaos has a niche application in such systems, it can be exploited for hardware security [41], but to our knowledge, it has not yet been reported in multi-particle experiments. (Chaos has been observed in single particle systems [42,43].) Our model predicts chaos, along with quasiperiodicity and reentrance, occurs for all $N > 1$ and gives parameter regimes where it is likely to arise, namely when the driving and interelement coupling have comparable magnitude and are large relative to the pinning $E/b \approx K/b, J/b \gg 1$. The model or a close variant may also be useful in studies of charge density waves which couple to lattice vibrations [44]. Equation (2) for $\dot{\theta}_i$ has already been used to model the phase of the charge wave [22,25,26]; the novelty would be Eq. (1) for \dot{x}_i which could represent the displacements of the lattice atoms from their equilibrium positions. Such displacements form sinusoidal patterns [44], encapsulated by the $b \sin(x_i - \beta_i)$ term, which competes with the tendency to “synchronize” at equilibrium $x_i = x_j = 0$, as per the $K \sin(x_j - x_i)$ term.

Code used for simulations and analytic calculations is available at github [45].

APPENDIX A: $J = -K$ COUPLING

Our model is

$$\dot{x}_1 = E - b \sin(x_1 - \alpha_1) + \frac{J}{2} \sin(x_2 - x_1) \cos(\theta_2 - \theta_1), \quad (A1)$$

$$\dot{x}_2 = E - b \sin(x_2 - \alpha_2) - \frac{J}{2} \sin(x_2 - x_1) \cos(\theta_2 - \theta_1), \quad (A2)$$

$$\dot{\theta}_1 = E - b \sin(\theta_1 - \beta_1) + \frac{K}{2} \sin(\theta_2 - \theta_1) \cos(x_2 - x_1), \quad (A3)$$

$$\dot{\theta}_2 = E - b \sin(\theta_2 - \beta_2) - \frac{K}{2} \sin(\theta_2 - \theta_1) \cos(x_2 - x_1). \quad (A4)$$

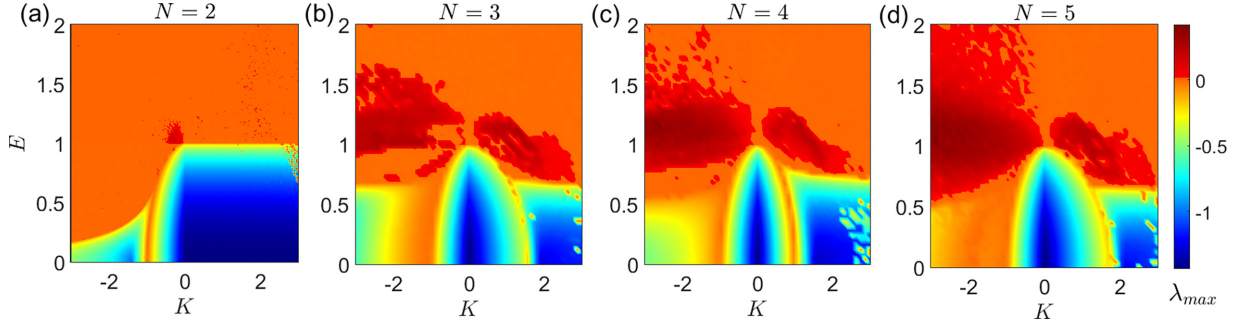


FIG. 10. Comparison of $N = 2, 3, 4, 5$ for $J = K$. As N increases, the shape starts to change. At $N = 5$ the shape is almost identical to that of the $N = \infty$ results, plotted in Fig. 11 below for convenience.

Defining the difference and sum coordinates

$$x_{\pm} = \frac{x_1 \pm x_2}{2}, \quad (\text{A5})$$

$$\theta_{\pm} = \frac{\theta_1 \pm \theta_2}{2}, \quad (\text{A6})$$

and setting $(\alpha_1, \alpha_2) = (\beta_1, \beta_2) = (0, \pi)$, $b = 1$, and $J = -K$, we get

$$\dot{x}_+ = E - \cos x_+ \sin x_-, \quad (\text{A7})$$

$$\dot{x}_- = -\sin x_+ \cos x_- + \frac{K}{2} \sin 2x_- \cos 2\theta_-, \quad (\text{A8})$$

$$\dot{\theta}_+ = E - \cos \theta_+ \sin \theta_-, \quad (\text{A9})$$

$$\dot{\theta}_- = -\sin \theta_+ \cos x_- - \frac{K}{2} \sin 2\theta_- \cos 2x_-, \quad (\text{A10})$$

presented in the main text. To solve for the fixed points, we first eliminate (x_-, θ_-) using Eqs. (A7) and (A9),

$$\sin x_- = E \sec x_+, \quad (\text{A11})$$

$$\sin \theta_- = E \sec \theta_+. \quad (\text{A12})$$

Subbing these into Eqs. (A8) and (A10), we get

$$\sqrt{1 - E^2 \sec^2 x_+} (EK \sec x_+ (2E^2 \sec^2 \theta_+ - 1) - \sin x_+) = 0, \quad (\text{A13})$$

$$\sqrt{1 - E^2 \sec^2 \theta_+} (EK \sec \theta_+ (2E^2 \sec^2 x_+ - 1) - \sin \theta_+) = 0. \quad (\text{A14})$$

These have the form $AB = CD = 0$ which implies four different fixed points defined by (A, C) , (A, D) , (B, C) , (B, D) being $(0,0)$ individually.

a. Half-pinned state

This state is defined by a symmetric pair of fixed points: when x_i stay pinned and θ_i sync, or the reverse. In the above notation, these correspond to $(A, D) = (0, 0)$ and $(B, D) = (0, 0)$. We study the $(A, D) = (0, 0)$ without loss of generality, given by

$$\sqrt{1 - E^2 \sec^2 x_+} = 0, \quad (\text{A15})$$

$$\sqrt{1 - E^2 \sec^2 \theta_+} (EK \sec \theta_+ (2E^2 \sec^2 x_+ - 1) - \sin \theta_+) = 0. \quad (\text{A16})$$

Mathematica finds 32 solutions to these, of which 4 are stable. These 4 fixed points have the form

$$x_+ = -\cos^{-1}(-E), \quad (\text{A17})$$

$$x_- = -\frac{\pi}{2}, \quad (\text{A18})$$

$$\theta_+ = \cos^{-1} \left(-\frac{\sqrt{1 - \sqrt{1 - 4E^2 K^2}}}{\sqrt{2}} \right), \quad (\text{A19})$$

$$\theta_- = -\sin^{-1} \left(\frac{\sqrt{2}E}{\sqrt{1 - \sqrt{1 - 4E^2 K^2}}} \right). \quad (\text{A20})$$

Finding the stability of these is harder. The Jacobian matrix yields eigenvalues

$$\lambda_1 = -\sqrt{1 - E^2}, \quad (\text{A21})$$

$$\lambda_2 = \frac{\sqrt{1 - 4E^2 K^2} - K(\sqrt{1 - E^2} + K) + 1}{K}, \quad (\text{A22})$$

$$\lambda_3 = \frac{1}{2} \left(-\frac{2E\sqrt{\sqrt{1 - 4E^2 K^2} + 1}}{\sqrt{1 - \sqrt{1 - 4E^2 K^2}}} - \frac{\sqrt{1 - 4E^2 K^2} + \frac{\sqrt{K^2(8E^2\sqrt{1 - 4E^2 K^2} - K^2(\sqrt{1 - 4E^2 K^2} + 16E^2 - 1) - 4\sqrt{1 - 4E^2 K^2} + 4)}}{\sqrt{1 - \sqrt{1 - 4E^2 K^2}}} + 1}{K} + K \right), \quad (\text{A23})$$

$$\lambda_4 = \frac{1}{2} \left(-\frac{2E\sqrt{\sqrt{1-4E^2K^2}+1}}{\sqrt{1-\sqrt{1-4E^2K^2}}} - \frac{\sqrt{1-4E^2K^2} - \frac{\sqrt{K^2(8E^2\sqrt{1-4E^2K^2}-K^2(\sqrt{1-4E^2K^2+16E^2-1})-4\sqrt{1-4E^2K^2+4})}}{\sqrt{1-\sqrt{1-4E^2K^2}}} + 1}{K} + K \right). \quad (\text{A24})$$

Solving $\lambda_3 = 0$ and removing the square roots by successive squaring leads to

$$4E^4(2EK-1)(2EK+1)(E^2+K^2-1) \times ((2E^2K+K)^2+3(E^2-1)) = 0. \quad (\text{A25})$$

The relevant branch is

$$E_{c2} = -\frac{1}{2K}. \quad (\text{A26})$$

Solving $\lambda_2 = 0$ gives us the other part of the boundary

$$E_{c3} = \frac{\sqrt{-K^4+5K^2-4}}{3K}. \quad (\text{A27})$$

We again observe zero eigenvalue bifurcation on the boundary.

b. Sync state

The final fixed point is $(B, D) = (0, 0)$,

$$EK \sec x_+ (2E^2 \sec^2 \theta_+ - 1) - \sin x_+ = 0, \quad (\text{A28})$$

$$EK \sec \theta_+ (2E^2 \sec^2 x_+ - 1) - \sin \theta_+ = 0. \quad (\text{A29})$$

Mathematica struggles to solve these, so we have to do them by hand. First, isolate $\sec \theta_+$ from the top equation,

$$\sec \theta_+ = \frac{\sqrt{EK - \sin x_+ \cos x_+}}{\sqrt{2E^{3/2}\sqrt{K}}}. \quad (\text{A30})$$

Then substitute this into the second equation after swapping $\sin \theta_+ = (1 - 1/\sec^2 \theta_+)^{-1/2}$ to find

$$-\sqrt{K}\sqrt{2EK - \sin(2x_+)} - 2\sqrt{E}\sqrt{\frac{4E^3K}{\sin(2x_+) - 2EK} + 1} + 2E^2\sqrt{K}\sec^2(x_+)\sqrt{2EK - \sin(2x_+)} = 0. \quad (\text{A31})$$

We remove the square roots by isolating each one on the LHS, squaring, then repeating the process. A gigantic equation in $\cos x_+$, $\sin x_+$, $\tan x_+$ results. Setting $c := \sqrt{\cos x_+}$ and simplifying however results in a product of a third and fourth order polynomials

$$P_3(c)P_4(c) = 0, \quad (\text{A32})$$

where

$$P_3(c) = -c^3 + c^4 + c^2E^2K^2 - 4cE^4K^2 + 4E^6K^2, \quad (\text{A33})$$

$$P_4(c) = c^4K^2 + c^3(-8E^2K^2 - K^2) + c^2(E^2K^4 + 16E^4K^2 + 4E^2K^2 + 4E^2) + c(-4E^4K^4 - 8E^4K^2) + 4E^6K^4. \quad (\text{A34})$$

Recalling $\cos x_+ = c^2$, we see x_+ will be a simple transformation of the roots of cubics and quartics—known, but ugly. These constitute a large family of fixed points. To find the relevant ones, we plotted them and found

$$x_+ = \sec^{-1} \left(-\frac{2}{\sqrt{8E^2 + \frac{S_2}{K} - S_1 + 1}} \right), \quad (\text{A35})$$

$$x_- = -\sin^{-1} \left(\frac{2E}{\sqrt{8E^2 + \frac{S_2}{K} - S_1 + 1}} \right), \quad (\text{A36})$$

$$\theta_+ = -\cos^{-1} \left(\frac{2\sqrt{2}E^{3/2}\sqrt{K}}{\sqrt{\sqrt{-\frac{(8E^2K-KS_1+K+S_2)(S_2-K(-8E^2+S_1+3))}{K^2} + 4EK}}} \right), \quad (\text{A37})$$

$$\theta_- = \csc^{-1} \left(\frac{2\sqrt{2}\sqrt{E}\sqrt{K}}{\sqrt{\sqrt{-\frac{(8E^2K-KS_1+K+S_2)(S_2-K(-8E^2+S_1+3))}{K^2} + 4EK}}} \right), \quad (\text{A38})$$

where

$$S_1 = \sqrt{64E^4 - \frac{8E^2(K(K^2-2)(\sqrt{K^2-16E^2}+K)+2)}{K^2}} + \frac{2\sqrt{K^2-16E^2}}{K} + 2, \quad (\text{A39})$$

$$S_2 = \sqrt{K^2 - 16E^2}. \quad (\text{A40})$$

Calculating the stability of these was another monster. We derived the characteristic equation which has form

$$a_4 + a_3\lambda + a_2\lambda^2 + a_1\lambda^3 + a_0\lambda^4 = 0, \tag{A41}$$

where $a_i = f_i(E, K)$ where f were complicated functions:

$$a_0 = 1, \tag{A42}$$

$$a_1 = \frac{2\sqrt{1 - E^2S_4^2}}{S_4} + 2E\sqrt{1 - \frac{1}{S_3^2}S_3}, \tag{A43}$$

$$a_2 = \frac{K^2(S_4^4(- (1 - 2E^2S_3^2)^2) + 4S_4^2 - 4)}{S_4^4} + \frac{K(S_4^2 - 2)(2E^2S_3^2 - 1)(\sqrt{1 - E^2S_4^2} - E\sqrt{1 - \frac{1}{S_3^2}S_3S_4})}{S_4^3} + \frac{4E\sqrt{1 - \frac{1}{S_3^2}S_3}\sqrt{1 - E^2S_4^2}}{S_4} + E^2S_3^2 - E^2S_4^2 - \frac{1}{S_3^2} + \frac{1}{S_4^2}, \tag{A44}$$

$$a_3 = - \left[K^2S_3^2(S_4^4(1 - 2E^2S_3^2)^2 - 4S_4^2 + 4) \left(\sqrt{1 - E^2S_4^2} + E\sqrt{1 - \frac{1}{S_3^2}S_3S_4} \right) + K(S_4^2 - 2)S_4(2E^2S_3^2 - 1)(S_3^2 + S_4^2)(E^2S_3^2S_4^2 - 1) + 2S_4^3 \left(E^3\sqrt{1 - \frac{1}{S_3^2}S_3^3S_4^4} - E^2S_3^3S_4\sqrt{1 - E^2S_4^2} + S_4\sqrt{1 - E^2S_4^2} - E\sqrt{1 - \frac{1}{S_3^2}S_3^3} \right) \right] / S_3^2S_4^5, \tag{A45}$$

$$a_4 = - \left[-E^2S_4^2(S_4^4(KS_4^2\sqrt{1 - E^2S_4^2} - 2K\sqrt{1 - E^2S_4^2} + S_4) + 2KS_3^2(S_4^2 - 2)\sqrt{1 - E^2S_4^2} + S_4^5) + EK\sqrt{1 - \frac{1}{S_3^2}S_3^3}(S_4^2 - 2)(KS_4^2\sqrt{1 - E^2S_4^2} - 2K\sqrt{1 - E^2S_4^2} + S_4) + S_4^2(KS_4^2\sqrt{1 - E^2S_4^2} - 2K\sqrt{1 - E^2S_4^2} + S_4) + 2E^5K\sqrt{1 - \frac{1}{S_3^2}S_3^5S_4^4}(2KS_3^2\sqrt{1 - E^2S_4^2} + S_4^3 - 2S_4) + E^4S_3^4S_4^2(2KS_3^2S_4^2\sqrt{1 - E^2S_4^2} - 4KS_3^2\sqrt{1 - E^2S_4^2} + S_4^5) - E^3K\sqrt{1 - \frac{1}{S_3^2}S_3^3S_4}(2S_3^2(2KS_3^3\sqrt{1 - E^2S_4^2} + S_4^2 - 2) + (S_4^2 - 2)S_4^4) \right] / S_3^2S_4^5, \tag{A46}$$

where S_3 and S_4 are given by

$$S_3 = \frac{2}{\sqrt{8E^2 + \frac{S_2}{K} - S_1 + 1}}, \tag{A47}$$

$$S_4 = \frac{2\sqrt{2}\sqrt{E}\sqrt{K}}{\sqrt{\sqrt{-\frac{(8E^2K - KS_1 + K + S_2)(S_2 - K(-8E^2 + S_1 + 3))}{K^2}} + 4EK}}. \tag{A48}$$

The λ 's were findable in theory, but too complex to derive any meaningful stability information from. So instead checked the stability with the help of the Routh Hurwitz conditions:

$$a_0 > 0, \tag{A49}$$

$$a_1 > 0, \tag{A50}$$

$$a_1a_2 - a_0a_3 > 0, \tag{A51}$$

$$(a_1a_2 - a_0a_3)a_3 - a_1^2a_4 > 0, \tag{A52}$$

$$a_4 > 0. \tag{A53}$$

We found that the sync state solutions Eqs. (A35)–(A38) are stable whenever they exist. They exist when the terms inside the square root in the expressions of S_1 and S_2 in Eqs. (A39) and (A40) are greater or equal to zero. This gives us the stability and existence boundaries of the sync state quoted in the main text,

$$E_{c4} = \frac{K}{4}, \tag{A54}$$

$$E_{c5} = \frac{1}{2}\sqrt{\frac{K(\sqrt{K^2 - 4} + K) - 1}{K^2}}. \tag{A55}$$

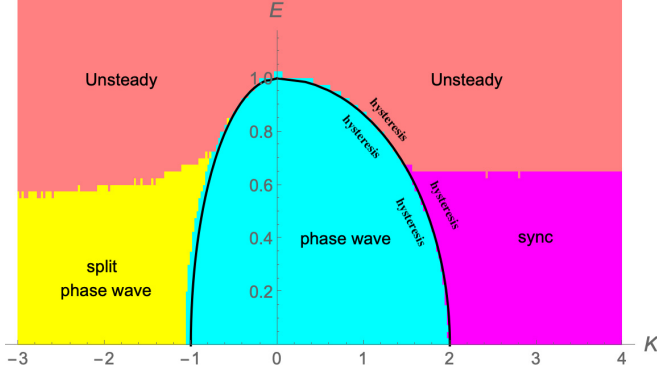


FIG. 11. Bifurcation diagram: $N \gg 1$ for $J = K$. We take $N = 100$ here. We refer the reader to Ref. [34] for details.

APPENDIX B: $J = +K$ COUPLING

The analysis here is the same dance as above, but surprisingly it gets easier. The governing equations read

$$\dot{x}_+ = E - \cos x_+ \sin x_-, \quad (\text{B1})$$

$$\dot{x}_- = -\sin x_+ \cos x_- - \frac{K}{2} \sin 2x_- \cos 2\theta_-, \quad (\text{B2})$$

$$\dot{\theta}_+ = E - \cos \theta_+ \sin \theta_-, \quad (\text{B3})$$

$$\dot{\theta}_- = -\sin \theta_+ \cos x_- - \frac{K}{2} \sin 2\theta_- \cos 2x_-. \quad (\text{B4})$$

$$\lambda_3 = \frac{1}{2} \left(-\frac{\sqrt{K^2(-K^2(16E^2+S_3-1)+8E^2S_3-4S_3+4)}}{\sqrt{1-S_3}} + S_3 + 1 - \frac{2E\sqrt{S_3+1}}{\sqrt{1-S_3}} + K \right), \quad (\text{B11})$$

$$\lambda_4 = \frac{1}{2} \left(-\frac{\sqrt{K^2(-K^2(16E^2+S_3-1)+8E^2S_3-4S_3+4)}}{\sqrt{1-S_3}} + S_3 + 1 - \frac{2E\sqrt{S_3+1}}{\sqrt{1-S_3}} + K \right), \quad (\text{B12})$$

where

$$S_3 = \sqrt{1 - 4E^2K^2}, \quad (\text{B13})$$

$$S_4 = \sqrt{K^2(8E^2\sqrt{1 - 4E^2K^2} - K^2(\sqrt{1 - 4E^2K^2} + 16E^2 - 1) - 4\sqrt{1 - 4E^2K^2} + 4)}. \quad (\text{B14})$$

Finally, the stability boundary is found as

$$E_{c6} = -\frac{1}{2K}. \quad (\text{B15})$$

At this boundary saddle node infinite period (SNIPER) bifurcation takes place which results into a periodic orbit; see Fig. 4. The black curves are the analytically calculated stability boundaries.

There are four fixed points like last time, but only the pinned and half-pinned are stable. We have already discussed the pinned state in the main text.

a. Half-pinned

Here the fixed points are

$$x_+ = \cos^{-1}(-E), \quad (\text{B5})$$

$$x_- = -\frac{\pi}{2}, \quad (\text{B6})$$

$$\theta_+ = \sec^{-1} \left(-\frac{\sqrt{2}}{\sqrt{1 - \sqrt{1 - 4E^2K^2}}} \right), \quad (\text{B7})$$

$$\theta_- = \sin^{-1} \left(\frac{\sqrt{2}E}{\sqrt{1 - \sqrt{1 - 4E^2K^2}}} \right). \quad (\text{B8})$$

We calculate the eigenvalues at this fixed point as

$$\lambda_1 = -\sqrt{1 - E^2}, \quad (\text{B9})$$

$$\lambda_2 = -\frac{K(\sqrt{1 - E^2} - K) + S_3 + 1}{K}, \quad (\text{B10})$$

APPENDIX C: $N > 2$ LIMIT FOR $J = K$ COUPLING

We increase the number of swarmsalators for the $J = K$ case and observe the bifurcation structure with the help of λ_{\max} in Fig. 10. It shows that when N increases, the chaotic region (dark red) also expands. Eventually, in the $N \rightarrow \infty$ limit, we get the bifurcation diagram delineated in Fig. 11.

- [1] D. A. Allwood, G. Xiong, C. Faulkner, D. Atkinson, D. Petit, and R. Cowburn, *Science* **309**, 1688 (2005).
 [2] Z. Luo, A. Hrabec, T. P. Dao, G. Sala, S. Finizio, J. Feng, S. Mayr, J. Raabe, P. Gambardella, and L. J. Heyderman, *Nature (London)* **579**, 214 (2020).

- [3] R. Wiesendanger, *Nat. Rev. Mater.* **1**, 16044 (2016).
 [4] C. Reichhardt, C. J. O. Reichhardt, and M. V. Milošević, *Rev. Mod. Phys.* **94**, 035005 (2022).
 [5] L. H. Reddy, J. L. Arias, J. Nicolas, and P. Couvreur, *Chem. Rev.* **112**, 5818 (2012).

- [6] T.-H. Yang, S. Zhou, K. D. Gilroy, L. Figueroa-Cosme, Y.-H. Lee, J.-M. Wu, and Y. Xia, *Proc. Natl. Acad. Sci. USA* **114**, 13619 (2017).
- [7] A. Bricard, J.-B. Caussin, D. Das, C. Savoie, V. Chikkadi, K. Shitara, O. Chepizhko, F. Peruani, D. Saintillan, and D. Bartolo, *Nat. Commun.* **6**, 7470 (2015).
- [8] M. Caleap and B. W. Drinkwater, *Proc. Natl. Acad. Sci. USA* **111**, 6226 (2014).
- [9] J. Li, O. E. Shklyaev, T. Li, W. Liu, H. Shum, I. Rozen, A. C. Balazs, and J. Wang, *Nano Lett.* **15**, 7077 (2015).
- [10] M. Pinto, P. Ramalho, N. Moreira, A. Gonçalves, O. Nunes, M. Pereira, and O. Soares, *Environ. Adv.* **2**, 100010 (2020).
- [11] R. Cheng, W. Huang, L. Huang, B. Yang, L. Mao, K. Jin, Q. ZhuGe, and Y. Zhao, *ACS Nano* **8**, 7746 (2014).
- [12] L. Manamanchaiyaporn, X. Tang, Y. Zheng, and X. Yan, *IEEE Robot. Autom. Lett.* **6**, 5605 (2021).
- [13] J. C. Slonczewski, *AIP Conf. Proc.* **5**, 170 (1972).
- [14] S. A. Nasser, E. Martinez, and G. Durin, *J. Magn. Magn. Mater.* **468**, 25 (2018).
- [15] E. Haltz, S. Krishnia, L. Berges, A. Mougin, and J. Sampaio, *Phys. Rev. B* **103**, 014444 (2021).
- [16] Z. T. Liu, Y. Shi, Y. Zhao, H. Chaté, X.-q. Shi, and T. H. Zhang, *Proc. Natl. Acad. Sci. USA* **118**, e2104724118 (2021).
- [17] A. Zöttl and H. Stark, *Annu. Rev. Condens. Matter Phys.* **14**, 109 (2023).
- [18] C. Sándor, A. Libal, C. Reichhardt, and C. J. Olson Reichhardt, *Phys. Rev. E* **95**, 032606 (2017).
- [19] C. Reichhardt and C. O. Reichhardt, *Rep. Prog. Phys.* **80**, 026501 (2017).
- [20] D. Levis, I. Pagonabarraga, and B. Liebchen, *Phys. Rev. Res.* **1**, 023026 (2019).
- [21] B. Liebchen and D. Levis, *Phys. Rev. Lett.* **119**, 058002 (2017).
- [22] S. H. Strogatz, C. M. Marcus, R. M. Westervelt, and R. E. Mirollo, *Physica D* **36**, 23 (1989).
- [23] K. O’Keeffe, S. Ceron, and K. Petersen, *Phys. Rev. E* **105**, 014211 (2022).
- [24] S. Yoon, K. P. O’Keeffe, J. F. F. Mendes, and A. V. Goltsev, *Phys. Rev. Lett.* **129**, 208002 (2022).
- [25] S. H. Strogatz, C. M. Marcus, R. M. Westervelt, and R. E. Mirollo, *Phys. Rev. Lett.* **61**, 2380 (1988).
- [26] S. H. Strogatz and R. M. Westervelt, *Phys. Rev. B* **40**, 10501 (1989).
- [27] H. Jin, J. Cui, and W. Zhan, *Langmuir* **39**, 4198 (2023).
- [28] J. Yan, M. Bloom, S. C. Bae, E. Luijten, and S. Granick, *Nature (London)* **491**, 578 (2012).
- [29] B. Zhang, A. Sokolov, and A. Snezhko, *Nat. Commun.* **11**, 4401 (2020).
- [30] S. Zhang, W. Wang, D. Burn, H. Peng, H. Berger, A. Bauer, C. Pfeleiderer, G. Van Der Laan, and T. Hesjedal, *Nat. Commun.* **9**, 2115 (2018).
- [31] A. Hrabec, V. Křížáková, S. Pizzini, J. Sampaio, A. Thiaville, S. Rohart, and J. Vogel, *Phys. Rev. Lett.* **120**, 227204 (2018).
- [32] A. Hoffmann, P. Prieto, and I. K. Schuller, *Phys. Rev. B* **61**, 6958 (2000).
- [33] See Supplemental Material at <http://link.aps.org/supplemental/10.1103/PhysRevE.109.044603> for movie demos of our experiments.
- [34] G. K. Sar, D. Ghosh, and K. O’Keeffe, *Phys. Rev. E* **107**, 024215 (2023).
- [35] Note, in Ref. [34] we called pinned and antipinned states the phase wave and split phase wave, respectively. These are tools from coupled oscillator theory we discussed in the Introduction.
- [36] I. Aihara, *Phys. Rev. E* **80**, 011918 (2009).
- [37] K. Chaudhary, J. J. Juárez, Q. Chen, S. Granick, and J. A. Lewis, *Soft Matter* **10**, 1320 (2014).
- [38] A. Das, J. K. Bhattacharjee, and T. R. Kirkpatrick, *Phys. Rev. E* **101**, 023103 (2020).
- [39] Y. Kuramoto, *Chemical Oscillations, Waves, and Turbulence* (Springer, Berlin, 1984).
- [40] M. Ledesma-Motolinía, J. L. Carrillo-Estrada, A. Escobar, F. Donado, and P. Castro-Villarreal, *Phys. Rev. E* **107**, 024902 (2023).
- [41] S. Ghosh, *Proc. IEEE* **104**, 1864 (2016).
- [42] Y. Chen, X. Ge, W. Luo, S. Liang, X. Yang, L. You, Y. Zhang, and Z. Yuan, *Phys. Rev. B* **107**, L020405 (2023).
- [43] L. Shen, J. Xia, X. Zhang, M. Ezawa, O. A. Tretiakov, X. Liu, G. Zhao, and Y. Zhou, *Phys. Rev. Lett.* **124**, 037202 (2020).
- [44] H. Hedayat, C. J. Sayers, D. Bugini, C. Dallera, D. Wolverson, T. Batten, S. Karbassi, S. Friedemann, G. Cerullo, J. van Wezel *et al.*, *Phys. Rev. Res.* **1**, 023029 (2019).
- [45] <https://github.com/Khev/swarmalators/tree/master/1D/on-ring/random-pinning>